

Microstructural evolution and dynamic strain aging (DSA) of Mg-6%Gd-1%Zn alloy during tension and compression testing at intermediate temperatures

Gerardo Garcés^{a,*}, Pablo Pérez^a, Rafael Barea^b, Bryan W. Chávez^b, Judit Medina^a, Paloma Adeva^a

^aDepartamento de Metalurgia Física, Centro Nacional de Investigaciones Metalúrgicas (CENIM, CSIC),
Avda. Gregorio del Amo 8, 28040, Madrid, Spain

^bDepartamento de Ingeniería Industrial, Universidad Nebrija, Campus Dehesa de la Villa,
C. Pirineos 55, 28040 Madrid (Spain)

*Corresponding author: Gerardo Garcés: ggarcés@cenim.csic.es

Submitted: 28 November 2017; Accepted: 3 July 2018; Available On-line: 31 August 2018

ABSTRACT: The Mg-6%Gd-1%Zn alloy exhibits flow serrations when strained at intermediate temperatures due to the dynamic strain ageing phenomenon. Such flow serrations during deformation need the simultaneous and competitive movement of diffusing solutes and mobile dislocations. Although the alloy examined has a random texture, tension-compression asymmetry and significantly greater yield stress and work hardening in compression than in tension have been observed. During deformation at intermediate temperatures, and independently of the nature of the stress (tension or compression), the activation of $\langle a \rangle$ -dislocations and tensile twin systems has been observed. The volume fraction of twins is always higher, however, in the case of compression testing. At the intermediate temperatures where flow serrations are observed, Gd and Zn atoms pin dislocations as well as twins. Above 250 °C, the flow serrations disappear and γ' and γ'' precipitates form in the basal plane which increase work hardening.

KEYWORDS: Dynamic strain aging; Magnesium alloys; Microstructural evolution; Twinning

Citation/Citar como: Garcés, G.; Pérez, P.; Barea, R.; Chávez, B.W.; Medina, J.; Adeva, P. (2018). "Microstructural evolution and dynamic strain aging (DSA) of Mg-6%Gd-1%Zn alloy during tension and compression testing at intermediate temperatures". *Rev. Metal.* 54(3): e124. <https://doi.org/10.3989/revmetalm.124>

RESUMEN: *Evolución microestructural y envejecimiento dinámico por deformación en la aleación Mg-6%Gd-1%Zn durante ensayos a tracción y compresión a temperaturas intermedias.* La aleación Mg-6%Gd-1%Zn muestra el fenómeno de serrado durante la deformación a temperaturas intermedias debido al proceso de envejecimiento dinámico provocado por la presencia de átomos de soluto en solución sólida y dislocaciones móviles. Aunque la aleación tiene una textura al azar, se observa un comportamiento diferente en tracción y en compresión. El límite elástico y el endurecimiento es mayor cuando la aleación se ensaya en compresión. Durante la deformación a temperaturas intermedias se ha observado la activación de dislocaciones tipo $\langle a \rangle$ y maclas de tensión, independientemente del signo de la carga. Sin embargo, la fracción en volumen de maclas es siempre mayor cuando el material se somete a compresión. A temperaturas intermedias, los átomos de Gd y Zn anclan tanto las dislocaciones como las maclas. Por encima de 250 °C, el fenómeno de serrado desaparece y la presencia de precipitados γ' y γ'' en el plano basal aumenta el endurecimiento.

PALABRAS CLAVE: Aleaciones de magnesio; Envejecimiento dinámico; Evolución microestructural; Maclado

ORCID ID: Gerardo Garcés (<https://orcid.org/0000-0002-6896-7475>); Pablo Pérez (<https://orcid.org/0000-0002-4218-2573>); Rafael Barea (<https://orcid.org/0000-0002-6784-6110>); Bryan W. Chávez (<https://orcid.org/0000-0002-8015-1153>); Judit Medina (<https://orcid.org/0000-0002-3898-0935>); Paloma Adeva (<https://orcid.org/0000-0002-9111-8893>)

Copyright: © 2018 CSIC. This is an open-access article distributed under the terms of the Creative Commons Attribution 4.0 International (CC BY 4.0) License.

1. INTRODUCTION

The addition of rare earth (RE) elements to magnesium overcomes some of the weaknesses that prevent the increased use of magnesium alloys as a structural material in the transport and aerospace industries. The mechanical strength and creep resistance of magnesium alloys containing RE elements are superior to those of present commercial systems due to the formation of thermally stable precipitates (He *et al.*, 2007; Zhu *et al.*, 2010; Yuan *et al.*, 2013; Wang *et al.*, 2015; Gavras *et al.*, 2016). The addition of rare earths elements can also improve the formability of magnesium alloys due to the randomization of the crystallographic texture (Ball and Prangnell, 1994; Stanford *et al.*, 2008; Hantzsche *et al.*, 2010; Griffiths, 2015) and the changes of the relative CRSSs induced by these elements (Herrera-Solaz, 2014; Hidalgo-Manrique *et al.*, 2017).

During plastic deformation at intermediate temperatures (100–250 °C), several binary and ternary magnesium alloys containing RE elements exhibit serrated flow (also known as the Portevin–Le Chatelier effect) (Couling, 1959; Zhu and Nie, 2004; Zhongjun *et al.*, 2007; Fang *et al.*, 2009; Gao *et al.*, 2009; Stanford *et al.*, 2010; Jiang *et al.*, 2011; Wu *et al.*, 2012; Yuan *et al.*, 2013; Cai *et al.*, 2014; Garcés *et al.*, 2015). Different explanations of this have been proposed depending on the strain rate of the mechanical tests. On one hand, the dynamic interaction between dislocations and diffusing solute atoms, known as dynamic strain ageing (DSA), is commonly accepted to explain the serrations observed at low strain rates. On the other hand, at high strain rates, the appearance of serrations has been related to the shearing of precipitates by dislocations.

DSA in magnesium alloys has mostly been studied during tensile testing. Serrated flow has also been reported, however, for other kinds of mechanical tests, such as compression and torsion testing (Christodoulou *et al.*, 2002; Humphreys *et al.*, 2003). Moreover, the influence of other types of deformation mechanism, such as twinning, on DSA has hardly been examined. Of special relevance may be the interaction between RE atoms and twins, since it is known that RE atoms segregate to twin boundaries during static thermal treatments of deformed samples (Nie *et al.*, 2013; Zhu *et al.*, 2017; Zhu *et al.*, 2018). Such segregation induces a strong pinning effect on twin boundaries, preventing further twin growth during subsequent loading (Nie *et al.*, 2013). In a similar way, Somekawa *et al.* (2017) also observed that the segregation of yttrium to twin boundaries led to a decrease in the damping capacity of binary Mg–Y alloys.

The present paper studies the DSA phenomenon in Mg–6%Gd–1%Zn alloy during both tension and compression testing at intermediate temperatures.

The microstructural evolution of solutionised alloy during tension and compression tests at 200 °C is analyzed at different strain levels to identify the deformation mechanism for each loading mode. Finally, the interaction between RE atoms and both dislocations and twins is examined using transmission electron microscopy.

2. MATERIALS AND EXPERIMENTAL PROCEDURE

The Mg–6%Gd–1%Zn (wt.%) alloy, named GZ61, was fabricated by casting. High purity Mg and Zn, and a Mg–20%Gd (wt.%) master alloy were melted at 800 °C in an electric resistance furnace and then cast by pouring the liquid into a cylindrical steel mould. The 42 mm diameter cast cylinder was homogenized at 350 °C for 24 h and subsequently extruded at 400 °C at an extrusion ratio of 36:1.

Cylindrical specimens of gauge diameter 3 mm and length in the gauge section 10 mm (for tensile testing) and 8 mm length and 4 mm diameter (for compressive testing) were machined from the extrusion bars for testing always along the extrusion direction. Machined samples were solutionised at 500 °C for 24 h, buried in magnesium oxide powder to minimize oxidation.

Both tensile and compressive tests were carried out at initial strain rate of $4 \times 10^{-4} \text{ s}^{-1}$ from room temperature to 300 °C. At 200 °C, additional tensile and compressive tests were performed changing the strain rate during the test from 10^{-3} to 10^{-4} s^{-1} .

Scanning electron microscopy (SEM), using an instrument equipped for the electron backscattered diffraction (EBSD) technique, and transmission electron microscopy (TEM) were used to characterize the microstructure and evaluate the texture of the material in both the as-solutionised state and after tensile and compressive deformation. For these studies a JSM 6500F scanning electron microscope working at 20 kV and a JEM 2010 transmission electron microscope working at 200 kV were used. The samples all have cylindrical symmetry with the perpendicular reference directions: LD (loading direction) and RD (radial direction). It is important to remember that the loading direction coincides with the extrusion axis. Specimens for TEM were prepared by electrolytic polishing using a mixture of 25% nitric acid and 75% methanol at -30 °C and a voltage of 20 V. The surface preparation of magnesium alloy samples for EBSD is particularly delicate and requires a final chemical etch (Keshavarz and Barnett, 2006).

In-situ synchrotron diffraction experiments were carried out to evaluate the evolution of the internal strains during the DSA phenomenon using the P07 beam line of PETRA III (DESY, Hamburg, Germany). Cylinders of $d = 5 \text{ mm}$ of diameter and $l = 10 \text{ mm}$ in length were deformed in a Bähr

805A/D dilatometer at 200 °C at a strain rate of 10^{-3} s^{-1} . The temperature was measured using a thermocouple welded to the sample, with the compression test performed under argon flow to minimize oxidation. The synchrotron radiation beam was positioned at the center of the sample with the gauge volume defined approximately by the beam section ($1 \times 1 \text{ mm}^2$) and the cylinder diameter. The diffraction patterns were recorded using an exposure time of 0.5 s by a Perkin-Elmer XRD 1622 flat panel detector with an array of 2048^2 pixels, with an effective pixel size of $200 \times 200 \mu\text{m}^2$. The wavelength of the beam was 0.0124 nm (100 kV). LaB_6 was used as a reference to calibrate the acquired diffraction spectra. The detector-to-sample distance was 1789 mm. 2θ diffraction patterns were obtained by azimuthal integration of the Debye-Scherrer rings about $\pm 5^\circ$ in the axial and radial direction. FIT2D software was used to analyse diffraction peaks using a Gaussian function to obtain the position of the diffraction peak as well as its integrated intensity. The elastic strain for each orientation can be calculated by the shift in the position of the diffraction peak, as:

$$\varepsilon_{hkl} = \frac{d_{hkl} - d_{0,hkl}}{d_{0,hkl}} \quad (1)$$

Where d_{hkl} and $d_{0,hkl}$ are the planar spacing of the hkl plane in the stressed and stress-free crystal. It is assumed that there is no residual stress before the compression tests and, therefore, $d_{0,hkl}$ can be considered as d_{hkl} at 0 MPa. The lattice spacing and the diffraction angle θ are related through Bragg's law:

$$d_{hkl} = \frac{\lambda}{2 \sin \theta_{hkl}} \quad (2)$$

3. RESULTS AND DISCUSSION

Figure 1 shows the microstructure of the solutionised GZ61 material. Grains are equiaxed and randomly oriented (Fig. 1b) with a mean grain size of 120 nm. No second phases were observed, such that the gadolinium and zinc are in solid solution in the magnesium matrix.

Tensile and compressive curves at temperatures between room temperature and 300 °C are shown in Fig. 2 (a-b). In tension, the alloy yields at a stress near 100 MPa, and then rapidly hardens during plastic straining up to around 250 MPa. In compression, the behaviour is similar but the yield stress and the work-hardening are greater than in tension. Disregarding the sense of the applied load, the yield stress is seen to decrease slightly as the test temperature increases from room temperature to 100 °C, and then remains almost constant up to 300 °C (Fig. 2c). Mechanical tests carried out at temperatures between 125 and 200 °C showed flow serrations. Figure 2d shows tension and compression tests at 200 °C in which the strain rate was changed from 10^{-3} to 10^{-4} s^{-1} . Negative strain rate sensitivity is always found, with the flow stress during the test increasing when the strain rate is decreased, and vice versa. This effect is typical of the DSA phenomenon. It is difficult to identify the beginning of serrations in the tension/compression curves because the magnitude of the stress drop is initially very low. For an easy comparison, Fig. 3 shows, separately, tension and compression tests at temperatures where fluctuations are observed (125–250 °C). Serration shape and magnitude depend on the test temperature, strain level and stress sign (tension or compression). Between 125 and 200 °C and at a strain rate of $4 \times 10^{-4} \text{ s}^{-1}$, the stress amplitude of serration increases with increasing test temperature. At 250 °C, however, the serrations are less pronounced than at 200 °C. Moreover, comparing tension and

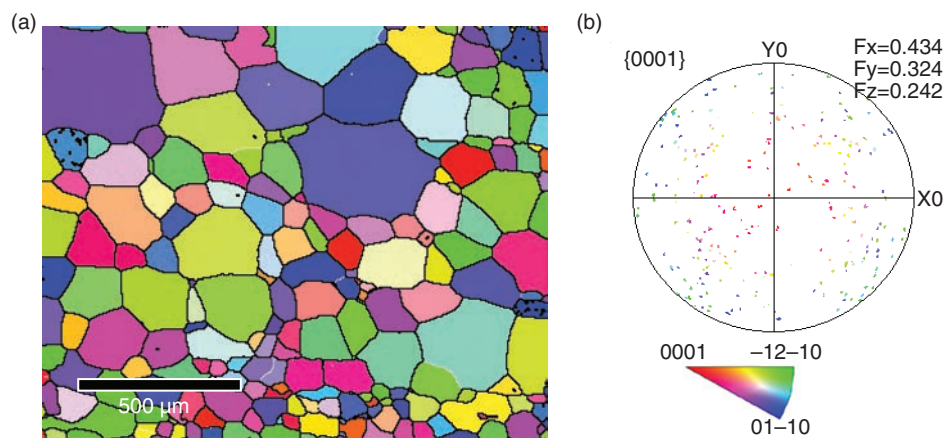


FIGURE 1. a) Orientation Image Map (OIM) of the GZ61 alloy after solution treatment; and b) (0002) pole figure obtained from EBSD of the GZ61 alloy.

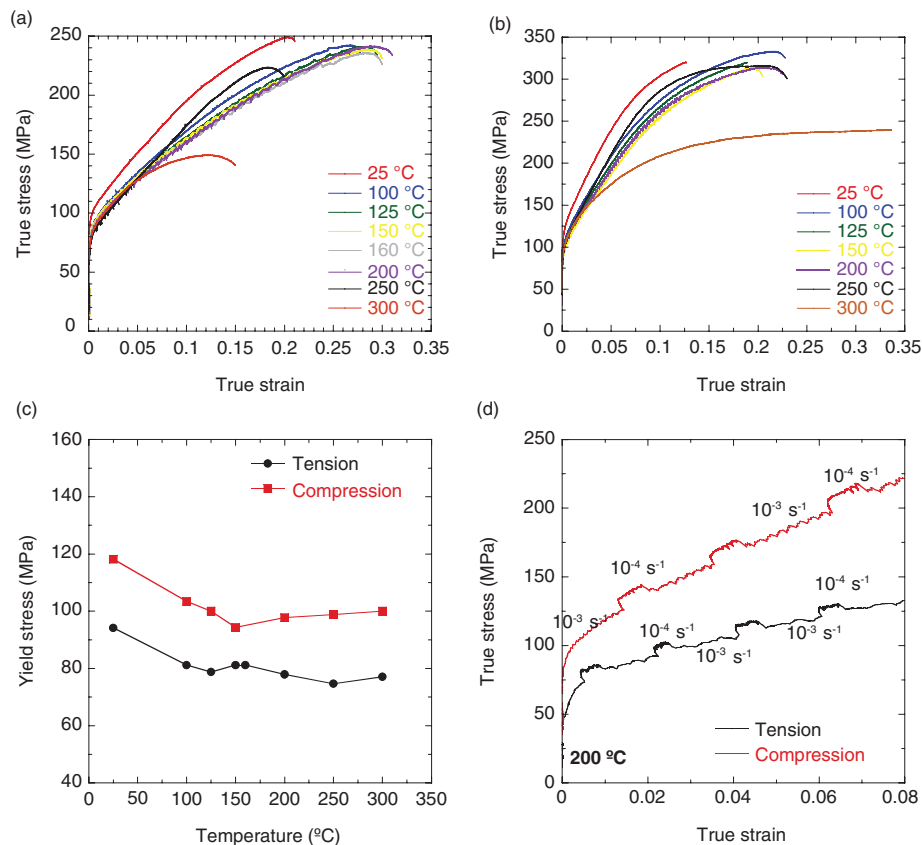


FIGURE 2. a) Tension and b) compression curves for the GZ61 alloy from room temperature up to 300 °C tested at a strain rate of $4 \times 10^{-4} \text{ s}^{-1}$; c) Evolution of the yield stress as a function of temperature during tension and compression tests; and d) Tension and compression tests at 200 °C with jumps in strain rates from 10^{-3} to 10^{-4} s^{-1} .

compression tests, the serration amplitude (in both stress and strain) is higher in tension (see Fig. 3f) than in compression. At 250 °C, the work hardening of the alloy after yielding is greater than for lower temperatures (except for room temperature testing), and independent of the stress sign. At 300 °C, however, in both tension and compression tests, the work-hardening and the maximum stress decrease markedly (see Fig. 2).

To understand the influence of the stress sign, tension or compression, on serrations, the microstructure and texture of the alloy have been studied in detail during plastic deformation at 200 °C using SEM and TEM. This test temperature was selected since the serration amplitude is the greatest during tensile and compressive testing (Fig. 3f). Figure 4 shows the evolution of the Orientation Image Mappings (OIMs) of the magnesium grains after strains of 2, 6, and 11%, and at the end of testing. The corresponding (0002) pole figures are also showed in Fig. 5. In general, for all strains, twins are clearly observed in tension and compression tests, although the volume fraction of twins is always higher in the compressed samples. Capek *et al.* (2017) have recently calculated the fraction of

grains having a particular Schmid factor for extension twinning in a polycrystalline magnesium alloy with random texture. The fraction of grains with high Schmid factor (between 0.4 and 0.5) is twice as high when the alloy is tested under compression. This conclusion agrees with the experimental observations here, i.e. a much higher volume fraction of twinned grains after compression testing.

The activation of tension twinning results in a rapid hardening after yielding (Kelley and Hosford, 1968; Capek *et al.*, 2017) which has usually been attributed to two effects. On the one hand, there is a composite strengthening effect associated with the reorientation of the twin from a soft to a hard orientation that inhibits the activation of either basal slip or tensile twinning (Reed-Hill, 1973). On the other hand, twin boundaries act as additional obstacles to subsequent slip and twinning deformation (Karaman *et al.*, 2000). Recently, El Kadiri and Oppedal (2010) proposed that the hardening is also related to a rapid increase in the dislocation density inside twins.

Above 6 % plastic strain, deformation and orientation gradients are observed within the grains, especially in grains where twins are not seen. These twin-free

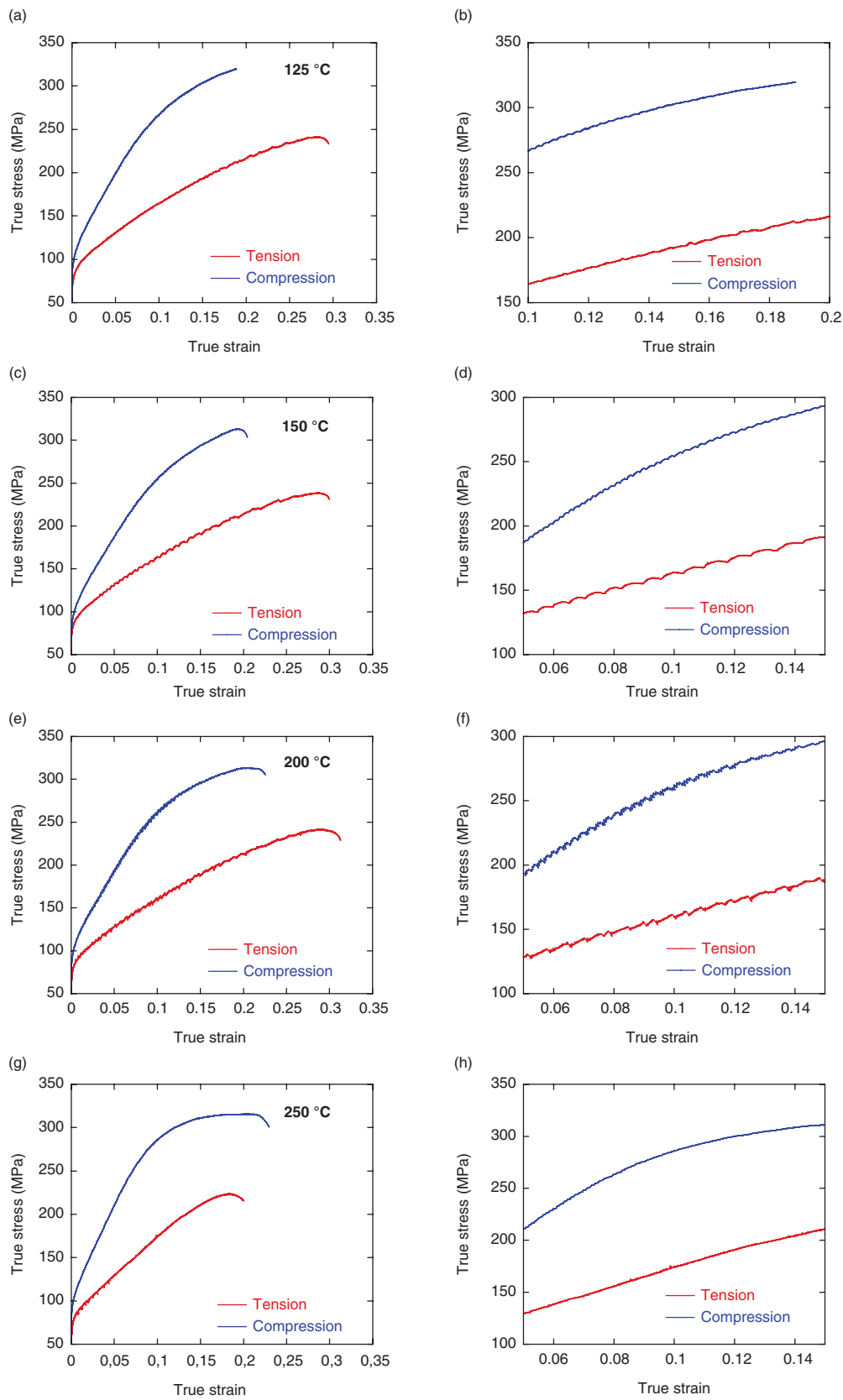


FIGURE 3. Tension and compression curves for the GZ61 alloy at a strain rate of $4 \times 10^{-4} \text{ s}^{-1}$ at (a, b) 125 °C, (c, d) 150 °C, (e, f) 200 °C and (g, h) 250 °C.

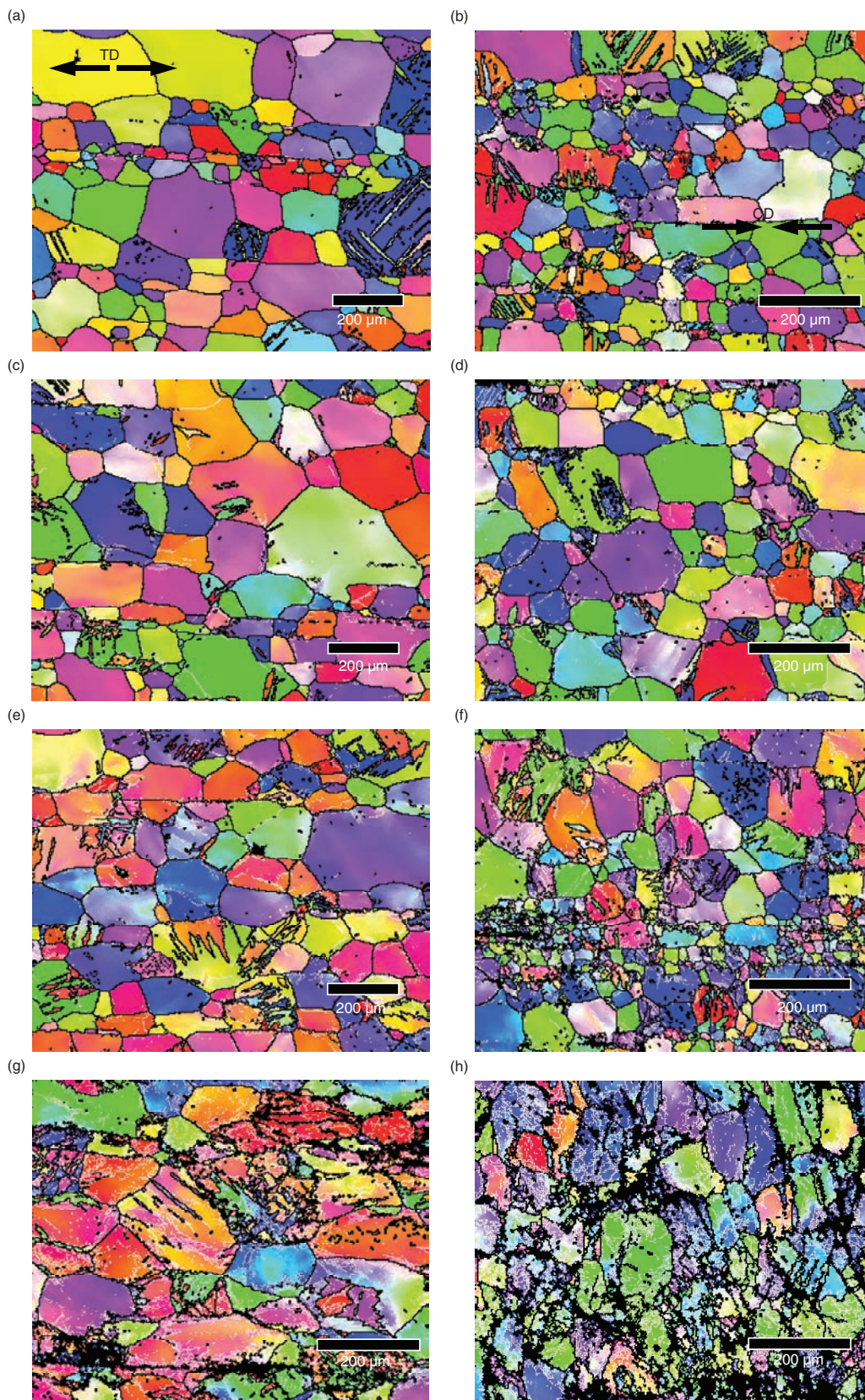


FIGURE 4. a) Orientation Image Map (OIM) of the GZ61 alloy at plastic strains of 2%, 6%, 11% and 20% in (a, c, e, g) tension and (b, d, f, h) compression. Load direction is marked for the case of 2% plastic strains and is the same for all other strain levels.

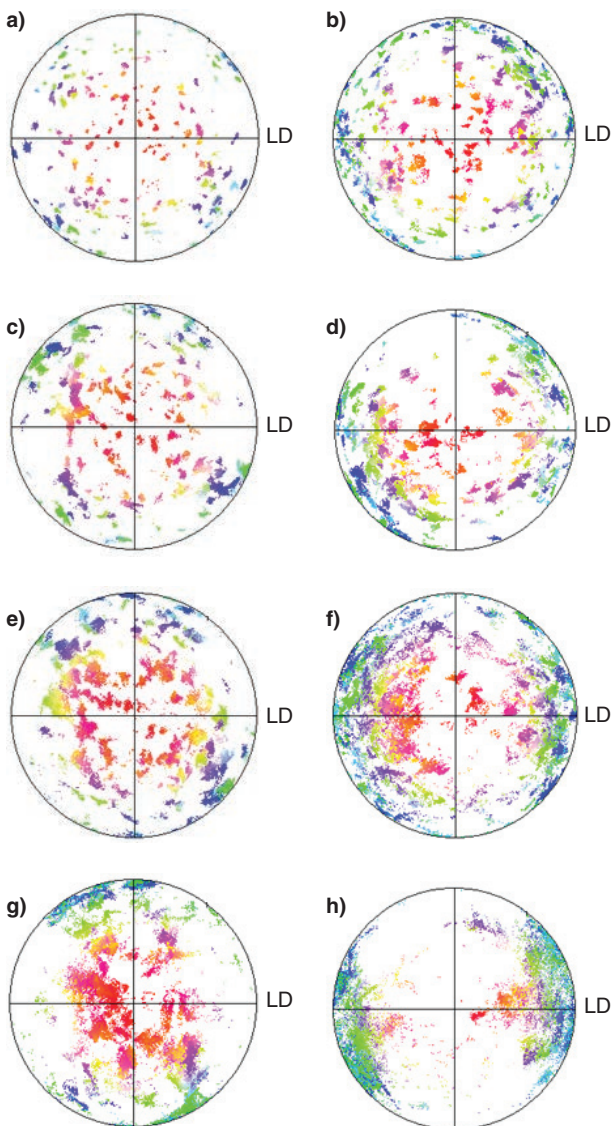


FIGURE 5. (0002) pole figure of the GZ61 alloy at 2%, 6%, 11% and 20% plastic strain in (a, c, e, g) tension and (b, d, f, h) compression.

grains deform by dislocation slip. This situation is also noticed in the (0002) pole figures (Fig. 5), where grain orientations are more widely spread, compared to the initial material (Fig. 1b), as the plastic strain increases. Low angle boundaries (white lines in Fig. 4) develop inside these grains at higher strain levels, as subgrains form. Moreover, many grains become oriented parallel to the stress direction, indicating that deformation is proceeding through the activation of basal slip (see Fig. 5d). This behaviour is not found in compressed samples (see Fig. 5h). In this case, most of the grains are perpendicular to the loading direction (LD) as a result of massive amounts of twinning. Figure 6 shows a detail of the twin boundaries in the sample tested to 6% plastic strain. For both tension and compression tests,

the twinning system is the tensile $\{10\bar{1}2\} \langle 10\bar{1}1 \rangle$ system which induces a rotation of 86° of the basal plane with respect to basal planes in parent grains (Fig. 6 e-f). Such tensile twinning is, in fact, the most common deformation twinning system reported in magnesium alloys.

The evolution of the internal strains has been evaluated using in-situ synchrotron radiation diffraction (SRD) during a compression test at 200°C at a strain rate of 10^{-3} s^{-1} : these are the same test parameters as for the samples analysed in Figs. 4-6. Figure 7a shows the Debye-Scherrer rings obtained before the compression test. After integration of the diffraction patterns as a function of 2θ are obtained (Fig. 7b). Owing to the random texture of the material, shown in Fig. 1b, the diffraction peak corresponding to the $\{10\bar{1}1\}$ planes exhibits the highest intensity when analysed in the axial direction. After compression testing, the intensity of the diffraction peaks changes significantly (Fig. 7c) in agreement with the pole figures of Fig. 5. The intensity of the (0002) diffraction peak has now strongly increased in the axial direction.

Changes in the interplanar spacing were evaluated for the $\{0002\}$, $\{10\bar{1}1\}$ and $\{10\bar{1}2\}$ diffraction peaks of the magnesium phase using equation 1 (Fig. 8a). The engineering stress-strain compression curve obtained during the diffraction experiment is also plotted, where serrated flow is clearly observed after yielding. This allows an easy comparison of overall sample strains and specific-planar strains. Fig. 8b shows the integrated intensity of the (0002) diffraction peak along the axial direction as a function of the applied stress. The evolution of the intensity of this (0002) diffraction peak can be used to give information about the activation of tensile twinning (Gharghouri *et al.*, 1999).

The evolution of the elastic strain of each family of grains exhibits a linear behavior until yielding of the particular family. The family of grains responsible for the beginning of macroscopic plasticity of the material is identified when the stress of the loss of elastic strain linearity (for the particular family) corresponds to the macroscopic yield stress. The macroscopic yield stress (defined as 0.2% of plastic deformation) during the in situ test is near 100 MPa, which agrees with the value estimated from the stress-strain curve in Fig. 2. At this stress, the internal strain corresponding to the (0002) diffraction peak loses its linearity and subsequently decreases (in absolute terms) in value. This inflexion in the elastic strain of the (0002) peak is related to a relaxation process during the initial stage of twinning (Garcés *et al.*, 2012a). Grains oriented with the basal plane perpendicular to the radial direction are under tension in the elastic regime. The formation of a “tensile” twin induces a rotation of 86° of the basal plane. It appears that the (0002) twins, perpendicular to the axial direction, which are initially

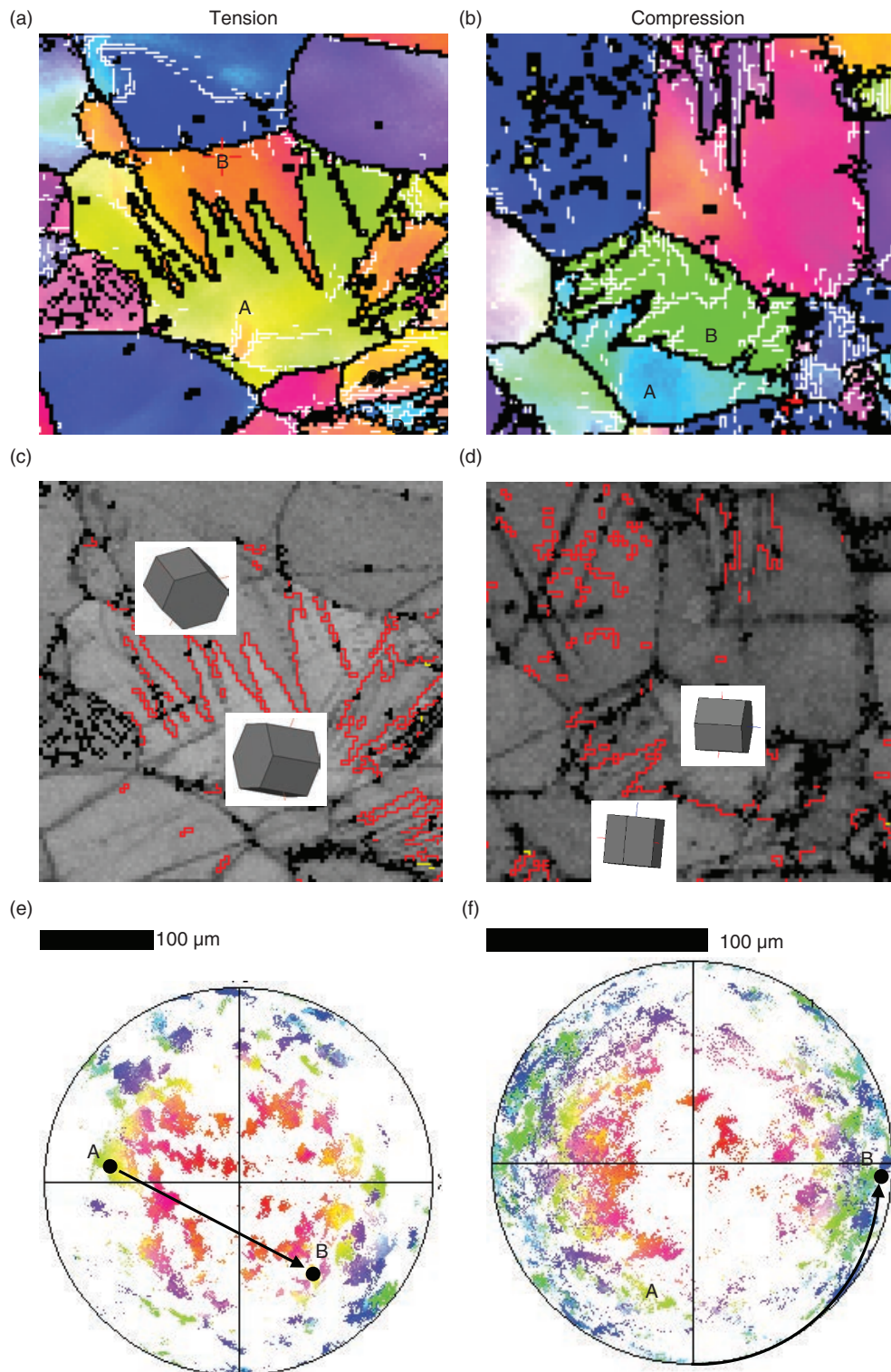


FIGURE 6. Orientation Image Maps (OIM) and $\{10\bar{1}2\}$ tensile twinning boundaries of the GZ61 alloy at 6% plastic strain in a, c) tension and b, d) compression. (0002) pole figure showing the rotation between the twin and the parent grain after e) tension and f) compression testing.

under tension require some relaxation time before adopting the compression load (Garcés *et al.*, 2012a). After further straining to reach a stress

of 125 MPa, the elastic strain of the (0002) peak decreases again rapidly to reach 175 MPa. Beyond this stress, the elastic strain shows little further

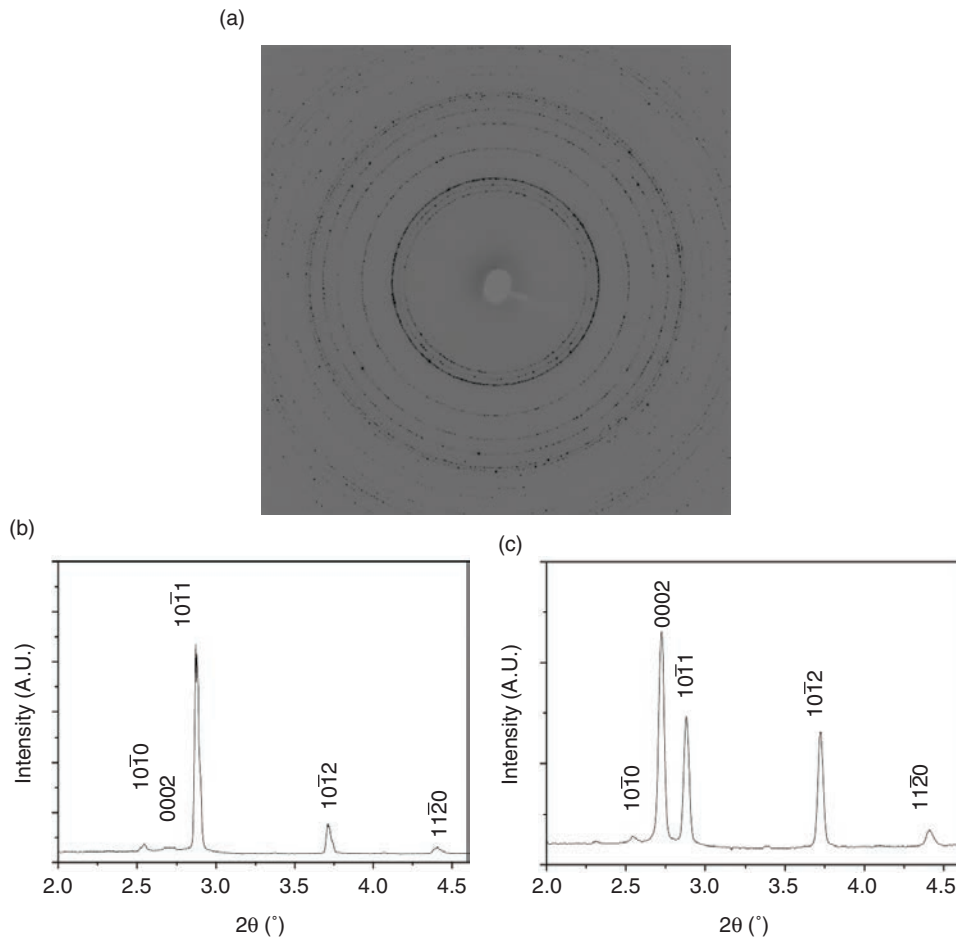


FIGURE 7. a) Synchrotron diffraction pattern recorded on the 2D detector obtained at 200 °C before compression; and b) Axial and c) radial diffraction patterns obtained from a) before compression.

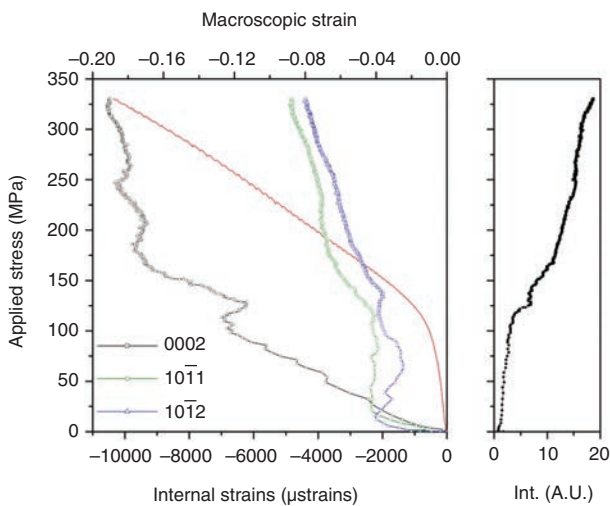


FIGURE 8. a) Evolution of the internal strains of {0002}, {1011} and {1012} diffraction peaks of the magnesium phase and macroscopic strain as a function of the applied stress; and b) Integrated intensity of the (0002) diffraction peak as a function of the applied stress.

change. Accompanying these changes of elastic strains, the intensity of the (0002) diffraction peak increases above the macroscopic yield stress, due to the formation and growth of twins.

It is interesting to point out that, for some diffraction peaks, the applied stress dependence of elastic strains loses linearity before reaching the macroscopic yield. This observation is usually related to micro-yielding (Agnew *et al.*, 2006; Garcés *et al.*, 2009). Grains with {1012} and {1011} planes perpendicular to the compression/axial axis deviate from linearity near a stress of 20 MPa. While these grains are favorably oriented for the easy activation of basal slip, it seems that these grains do not control macro-plasticity.

It should be noted that the internal strains and intensity seen in Fig. 8 exhibit fluctuations after macroscopic yielding. This is not common in previously published studies (Clausen *et al.*, 2008; Agnew *et al.*, 2013; Lentz *et al.*, 2015; Kada *et al.*, 2016). These fluctuations are therefore believed to be related to the DSA phenomena, with the increase in

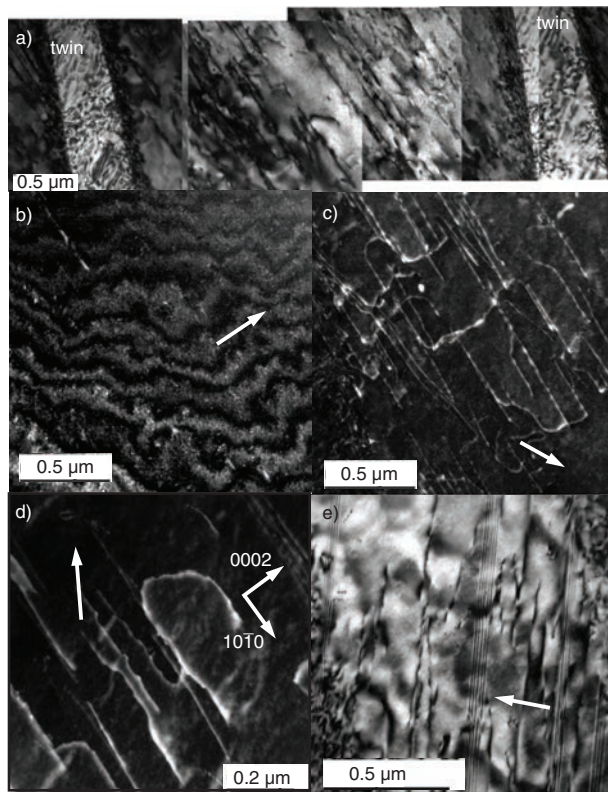


FIGURE 9. a) Bright field TEM images of the GZ61 alloy after tension testing to 2% plastic strain at 200 °C (zone axis $B=[1120]$). Weak beam images of the the GZ61 alloy after tension testing to 2% plastic strain at 200 °C (zone axis $B=[1120]$) with the b) 0002 and c) 1011 g vectors excited, respectively. d) Detail of dislocation structures in weak beam image ($B=[1120]$ and $g=1011$). e) Detail of a twin after 2% of plastic strain in tension ($B=[1120]$ and $g=0002$).

the volume fraction of twins taking place in “jumps” instead of continuously.

TEM samples were also examined at different strain levels, imposed in both tension and compression, to determine the deformation mechanisms occurring in the GZ61 material at intermediate temperatures. Figure 9a, shows the bright field image at the $B=[1120]$ zone axis of the alloy deformed in tension up to 2% strain. Dislocations and twins are observed within the magnesium grains. Analysis of these dislocation shows that they are invisible when the diffraction vector is $g=[0002]$ and visible when the diffraction vectors are $g=[1011]$ or $[10\bar{1}0]$ (Fig. 9 b-c, respectively). Therefore, it is expected that the Burgers vector of these dislocation is $\langle a \rangle$ -type. Moreover, dislocations are parallel to the $[0002]$ and $[10\bar{1}0]$ directions, such that it can be deduced that the slip of $\langle a \rangle$ dislocations occurs on both basal and non-basal planes during plastic deformation. These two kinds of dislocations interact, and are responsible for the DSA phenomenon due to dislocation locking by RE atoms. At higher magnification, the $\langle a \rangle$ dislocations are seen not to be straight, but

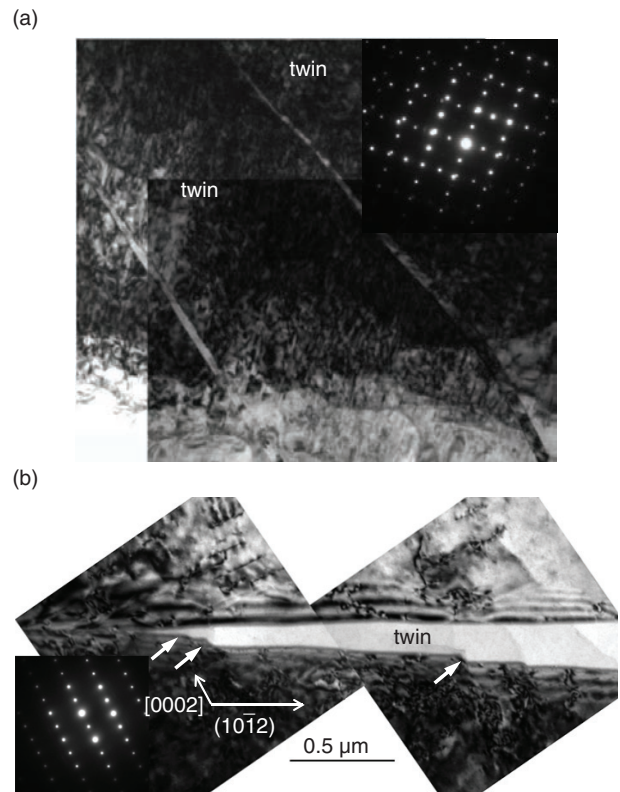


FIGURE 10. a) Bright field TEM images and SADP of the GZ61 alloy after compression testing to 6% plastic strain at 200 °C ($B=[1120]$); and b) White arrows show detail of a twin (zone axis of the matrix $B=[1120]$).

exhibit a wavy shape due to pinning of gadolinium atoms (Fig. 9d). Such interaction of RE atoms with dislocations promotes DSA since this leads to the temporary pinning of mobile dislocations.

Within twins, dislocations and basal stacking faults are also observed (Fig. 9e). Such stacking faults have been reported in Mg-RE-Zn alloys following thermal treatments and creep (Garcés *et al.*, 2012b; Zhu *et al.*, 2012) and are due to diffusion of RE and Zn atoms to faults produced by the slip of Shockley partial dislocations. Tomsett and Bevis (1969) and Wang and Agnew (2016) also reported that I_2 basal stacking faults result from the transmutation of $\langle a \rangle$ dislocations into $\langle c+a \rangle$ dislocations within the twins. The transmuted $\langle c+a \rangle$ dislocation discomposes into a $\langle c \rangle$ dislocation and two Shockley $1/3\langle 1\bar{1}00 \rangle$ dislocations (which produce the I_2 basal stacking faults). The absence of stacking faults in the parent grains deformed at 200 °C may lend support to this argument.

Figure 10 (a-b) shows the microstructure of a sample compressed to 6%, imaged in the $B=[1120]$ zone axis. Similar to the tensile samples, dislocations and twins are observed within magnesium grains. The selected area diffraction pattern (SAED) (Fig. 10a) clearly reveals the rotation of the crystal lattice in the twins, in agreement with the EBSD

maps of Fig. 6. The $\{10\bar{1}2\}$ twin boundary is faceted (see white arrows in Fig. 10b). This kind of faceted boundary has previously been reported as the basal-prismatic interface (Tu and Zhang, 2016). The size of these steps is around 50 nm, larger than those observed in other magnesium alloys. It is possible that the presence of RE and Zn atoms has an influence on twin growth. Nie *et al.* (2008) have demonstrated that there is segregation of gadolinium and zinc atoms to twin boundaries in compressed samples following static thermal treatments. Such segregation during straining would induce strong pinning of twin boundaries and inhibit twin growth. When DSA is observed during mechanical testing near 200 °C, the segregation process is dynamic or oscillatory, and the drag effect against twin boundary growth may be more heterogeneous than in the work of Nie *et al.* (2008).

During tension and compression testing at 250 °C, plate-shape particles precipitate on the basal plane of the magnesium grain in twins and in parent grains (Fig. 11 a-b). The diffuse streaks observed in SAD patterns along the [0002] direction are due to the high aspect ratio of the precipitates along the basal plane. The formation of g'' and g' precipitates in Mg-6%Gd-1%Zn-0.6%Zr alloy after annealing at 250 °C has been reported (Nie *et al.*, 2008; Li *et al.*, 2016). These precipitates are believed to have developed after twinning. If precipitates were generated before twinning, the misorientation between precipitates in the twinned and untwinned areas would be

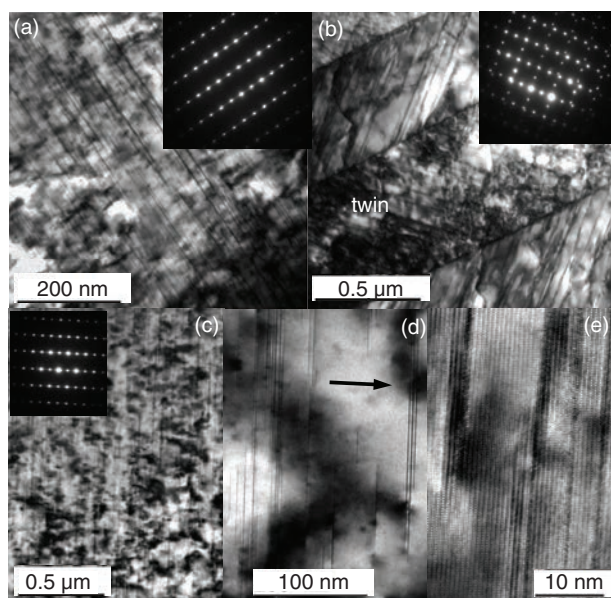


FIGURE 11. a, b) Bright field TEM images and SADP of the GZ61 alloy after tension testing to 2% plastic strain at 250 °C (B=[1120]); c) Bright field TEM images and SADP of the GZ61 alloy after tension testing to 2% plastic strain at 300 °C (B=[1120]); d) Detail of precipitates (B=[1120] and g=0002); e) HRTEM of γ' and γ'' precipitates (B=[1120]).

3.2 degrees (Geng *et al.*, 2011) with the twin engulfing the precipitate. Figure 11b shows that the orientation difference between precipitates in the twinned and untwinned area is 86 degrees, consistent with the post-twinning appearance of precipitates.

The presence of these precipitates is connected with the increase in the work hardening observed in the tension and compression tests at 250 °C. Geng *et al.* (2011) reported that the hardening that results from the formation of γ' precipitates is small at room temperature. At intermediate temperatures, however, the addition of small amounts of Zn improve the creep resistance of Mg-6Gd (Nie *et al.*, 2005), associated with the formation of a dense and uniform distribution of basal precipitate plates that are not found in the binary alloy.

Above 250 °C, the flow stress serrations disappear. Following the formation of γ'' and γ' precipitates, the Gd content dissolved in the magnesium matrix is reduced and the remaining Gd atoms are not sufficiently effective to lock either dislocations or twins. At 300 °C, γ'' precipitates, which are more effective for mechanical strengthening, transform to γ' which also grow along the [0002] direction (Fig. 9 c-e). The temperature is also sufficiently high for other deformation modes, notably dislocation climb, to occur such that strengthening is lost.

4. CONCLUSIONS

The evolution of microstructure in Mg-6%Gd-1%Zn during tension and compression tests at intermediate temperatures has been studied by SEM and TEM to explain the flow stress serrations observed during testing. The following conclusions have been drawn:

- The alloy presents flow serrations during tension and compression testing in the temperature range of 125–200 °C, which is related to the DSA phenomenon.
- Flow serrations are sensitive to the sign of the stress, tension or compression, and to the strain rate at the given temperature. The different activity of the deformation mechanisms, dislocation slip and twinning, in the alloy during straining at intermediate temperatures is responsible for this behavior.
- Solute atoms interact strongly with, and segregate to, both dislocations and twin boundaries. This leads to fluctuations in the evolution of the internal elastic strains during straining, as pinning-unpinning processes occur.
- Above 250 °C, the flow stress serrations disappear and g' and g'' precipitates form in the basal plane. Such precipitation induces a strong work hardening during plastic deformation at 250 °C.

ACKNOWLEDGEMENT

We should like to acknowledge financial support of the Spanish Ministry of Economy and Competitiveness under project number MAT2016-78850-R.

REFERENCES

- Agnew, S.R., Brown, D.W., Tomé, C.N. (2006). Validating a polycrystal model for the elastoplastic response of magnesium alloy AZ31 using in-situ neutron diffraction. *Acta Mater.* 54 (18), 4841–4852. <https://doi.org/10.1016/j.actamat.2006.06.020>.
- Agnew, S.R., Mulay, R.P., Polesak, F.J., Calhoun, C.A., Bhattacharyya, J.J., Clausen, B. (2013). In-situ neutron diffraction and polycrystal plasticity modeling of a Mg–Y–Nd–Zr alloy: Effects of precipitation on individual deformation mechanisms. *Acta Mater.* 61 (10), 3769–3780. <https://doi.org/10.1016/j.actamat.2013.03.010>.
- Ball, E.A., Prangnell, P.B. (1994). Tensile-compressive yield asymmetries in high strength wrought magnesium alloys. *Scripta Metall. Mater.* 31 (2), 111–116. [https://doi.org/10.1016/0956-716X\(94\)90159-7](https://doi.org/10.1016/0956-716X(94)90159-7).
- Cai, X., Fu, H., Guo, J., Peng, Q. (2014). Negative Strain-Rate Sensitivity of Mg Alloys Containing 18R and 14H Long-Period Stacking-Ordered Phases at Intermediate Temperatures. *Metall. Mater. Trans. A* 45 (9), 3703–3707. <https://doi.org/10.1007/s11661-014-2348-4>.
- Capek, J., Mathis, K., Clausen, B., Barnett, M. (2017). Dependence of twinned volume fraction on loading mode and Schmid factor in randomly textured magnesium. *Acta Mater.* 130, 319–328. <https://doi.org/10.1016/j.actamat.2017.03.017>.
- Christodoulou, N., Chow, C., Turner, P., Tomé, C., Klassen, R. (2002). Analysis of Steady-State Thermal Creep of Zr-2.5Nb Pressure Tube Material. *Metall. Mater. Trans. A* 33 (4), 1103–1115. <https://doi.org/10.1007/s11661-002-0212-4>.
- Clausen, B., Tomé, C.N., Brown, D.W., Agnew, S.R. (2008). Reorientation and stress relaxation due to twinning: Modeling and experimental characterization for Mg. *Acta Mater.* 56 (11), 2456–2468. <https://doi.org/10.1016/j.actamat.2008.01.057>.
- Couling, S.L. (1959). Yield points in a dilute magnesium-thorium alloy. *Acta Metall.* 7 (2), 133–134. https://ac.els-cdn.com/000161605990121X/1-s2.0-000161605990121X-main.pdf?_tid=7f605387-13bc-42a4-84b7-20b66f273f2f&acdnat=1530689365_46a9e777b153989b946b48fbcf25e6cf.
- El Kadiri, H., Oppedal, A.L. (2010). A crystal plasticity theory for latent hardening by glide twinning through dislocation transmutation and twin accommodation effects. *J. Mech. Phys. Solids* 58 (4), 613–624. <https://doi.org/10.1016/j.jmps.2009.12.004>.
- Fang, X.Y., Yi, D.Q., Nie, J.F. (2009). The serrated flow behaviour of Mg–Gd–(Mn–Sc) Alloys. *Metall. Mater. Trans. A* 40, 2761–2771. <https://doi.org/10.1007/s11661-009-9967-1>.
- Gao, L., Chen, R.S., Han, E.H. (2009). *Characterization of dynamic strain ageing in Mg-3.11wt.%Gd alloy*. R.A. Nyberg, S.R. Agnew, N.R. Neelameggham, M.O. Pekguleryuz (Eds.), Annual conference of TMS, San Francisco, USA, pp. 269–272.
- Garcés, G., Oñorbe, E., Pérez, P., Denks, I.A., Adeva, P. (2009). Evolution of internal strain during plastic deformation in magnesium matrix composites. *Mat. Sci. Eng. A-Struct.* 523 (1–2), 21–26. <https://doi.org/10.1016/j.msea.2009.06.026>.
- Garcés, G., Oñorbe, E., Pérez, P., Klaus, M., Genzel, C., Adeva, P. (2012a). Influence of SiC particles on compressive deformation of magnesium matrix composites. *Mat. Sci. Eng. A-Struct.* 533, 119–123. <https://doi.org/10.1016/j.msea.2011.10.103>.
- Garcés, G., Oñorbe, E., Dobes, F., Pérez, P., Antoranz, J.M., Adeva, P. (2012b). Effect of microstructure on creep behaviour of cast Mg97Y2Zn1 (at.%) alloy. *Mat. Sci. Eng. A-Struct.* 539, 48–55. <https://doi.org/10.1016/j.msea.2012.01.023>.
- Garcés, G., Muñoz-Morris, M.A., Morris, D.G., Pérez, P., Adeva P. (2015). An examination of strain ageing in a Mg–Y–Zn alloy containing Gd. *J. Mater. Sci.* 50 (17), 5769–5776. <http://dx.doi.org/10.1007/s10853-015-9124-8>.
- Gavras, S., Zhu, S.M., Nie, J.F., Gibson, M.A., Easton M.A. (2016). On the microstructural factors affecting creep resistance of die-cast Mg–La–rare earth (Nd, Y or Gd) alloys. *Mat. Sci. Eng. A-Struct.* 675, 65–75. <https://doi.org/10.1016/j.msea.2016.08.046>.
- Geng, J., Chun, Y.B., Stanford, N., Davies, C.H.J., Nie, J.F., Barnett, M.R. (2011). Processing and properties of Mg–6Gd–1Zn–0.6Zr: Part 2. Mechanical properties and particle twin interactions. *Mat. Sci. Eng. A-Struct.* 528 (10–11), 3659–3665. <https://doi.org/10.1016/j.msea.2011.01.024>.
- Gharghoury, M.A., Weatherly, G.C., Embury, J.D., Root, J. (1999). Study of the mechanical properties of Mg–7.7at.% Al by in-situ neutron diffraction. *Philos. Mag. A* 79 (7), 1671–1695. <https://doi.org/10.1080/01418619908210386>.
- Griffiths, D. (2015). Explaining texture weakening and improved formability in magnesium rare earth alloys. *Mater. Sci. Technol.* 31 (1), 10–24. <https://doi.org/10.1179/1743284714Y.00000000632>.
- Hantzschke, K., Bohlen, J., Wendt, J., Kainer, K.U., Yi, S.B., Letzig, D. (2010). Effect of rare earth additions on microstructure and texture development of magnesium alloy sheets. *Scripta Mater.* 63 (7), 725–730. <https://doi.org/10.1016/j.scriptamat.2009.12.033>.
- He, S.H., Zeng, X.Q., Peng, L.M., Gao, X., Nie, J.F., Ding, W.J. (2007). Microstructure and strengthening mechanism of high strength Mg–10Gd–2Y–0.5Zr alloy. *J. Alloys Compd.* 427 (1–2), 316–323. <https://doi.org/10.1016/j.jallcom.2006.03.015>.
- Herrera-Solaz, V., Hidalgo-Manrique, P., Pérez-Prado, M.T., Letzig, D., Llorca, J., Segurado, J. (2014). Effect of rare earth additions on the critical resolved shear stresses of magnesium alloys. *Mater. Lett.* 128, 199–203. <https://doi.org/10.1016/j.matlet.2014.04.144>.
- Hidalgo-Manrique, P., Robson, J.D., Pérez-Prado, M.T. (2017). Precipitation strengthening and reversed yield stress asymmetry in Mg alloys containing rare-earth elements: A quantitative study. *Acta Mater.* 124, 456–467. <https://doi.org/10.1016/j.actamat.2016.11.019>.
- Humphreys, A.O., Liu, D., Toroghinejad, M.R., Essadiqi, E., Jonas, J.J. (2003). Warm rolling behaviour of low carbon steels. *Mater. Sci. Technol.* 19 (6), 709–714. <https://doi.org/10.1179/026708303225002848>.
- Jiang, L., Jonas, J.J., Mishra, R. (2011). Effect of dynamic strain aging on the appearance of the rare earth texture component in magnesium alloys. *Mat. Sci. Eng. A-Struct.* 528 (21), 6596–6605. <https://doi.org/10.1016/j.msea.2011.05.027>.
- Kada, S.R., Lynch, P.A., Kimpton, J.A., Barnett, M.R. (2016). In-situ X-ray diffraction studies of slip and twinning in the presence of precipitates in AZ91 alloy. *Acta Mater.* 119, 145–156. <https://doi.org/10.1016/j.actamat.2016.08.022>.
- Karaman, I., Sehitoglu, H., Beaudoin, A.J., Chumlyakov, Y.I., Maier, H.J., Tomé, C.N. (2000). Modeling the deformation behaviour of hadfield steel single and polycrystals due to twinning and slip. *Acta Mater.* 48 (9), 2031–2047. [https://doi.org/10.1016/S1359-6454\(00\)00051-3](https://doi.org/10.1016/S1359-6454(00)00051-3).
- Kelley, E.W., Hosford, W.F. (1968). Plane-strain compression of magnesium and magnesium alloy crystals. *Trans. Metall. Soc. AIME* 242, 5–13.
- Keshavarz, Z., Barnett, M.R. (2006). EBSD analysis of deformation modes in Mg–3Al–1Zn. *Scripta Mater.* 55 (10), 915–918. <https://doi.org/10.1016/j.scriptamat.2006.07.036>.
- Lentz, M., Klaus, M., Wanger, M., Fahreson, C., Beyerlein, I.J., Zecevic, M., Reimers, W., Knezevic, M. (2015). Effect of age hardening on the deformation behavior of a Mg–Y–Nd alloy: In-situ X-ray diffraction and crystal plasticity modeling. *Mat. Sci. Eng. A-Struct.* 628, 396–409. <https://doi.org/10.1016/j.msea.2015.01.069>.

- Li, Z., Zheng, J., Chen, B. (2016). Unravelling the Structure of γ' in Mg-Gd-Zn: An Atomic-scale HAADF-STEM Investigation. *Mater. Charact.* 120, 345–348. <https://doi.org/10.1016/j.matchar.2016.08.011>.
- Nie, J.F., Gao, X., Zhu, S.M. (2005). Enhanced age hardening response and creep resistance of Mg-Gd alloys containing Zn. *Scripta Mater.* 53 (9), 1049–1053. <https://doi.org/10.1016/j.scriptamat.2005.07.004>.
- Nie, J.F., Oh-ishi, K., Gao, X., Hono, K. (2008). Solute segregation and precipitation in a creep-resistant Mg-Gd-Zn alloy. *Acta Mater.* 56 (20), 6061–6076. <https://doi.org/10.1016/j.actamat.2008.08.025>.
- Nie, J.F., Zhu, Y.M., Liu, J.Z., Fang, X.Y. (2013). Periodic Segregation of Solute Atoms in Fully Coherent Twin Boundaries. *Science* 340 (6135), 957–960. <https://doi.org/10.1126/science.1229369>.
- Reed-Hill, R.E. (1973). *Role of deformation twinning in determining the mechanical properties of metals: The Inhomogeneity of Plastic Deformation*. ASM International, Materials Park, OH, USA, p. 285.
- Stanford, N., Atwell, D., Beer, A., Davies, C., Barnett, M.R. (2008). Effect of microalloying with rare-earth elements on the texture of extruded magnesium-based alloys. *Scripta Mater.* 59 (7), 772–775. <https://doi.org/10.1016/j.scriptamat.2008.06.008>.
- Stanford, N., Sabirov, I., Sha, G., La Fontaine, A., Ringer, S., Barnett, M. (2010). Effect of Al and Gd Solutes on the Strain Rate Sensitivity of Magnesium Alloys. *Metall. Mater. Trans. A* 41 (3), 734–743. <https://doi.org/10.1007/s11661-009-0107-8>.
- Somekawa, H., Watanabe, H., Althaf Basha, D., Singh, A., Inoue T. (2017). Effect of twin boundary segregation on damping properties in magnesium alloy. *Scripta Mater.* 129, 35–38. <https://doi.org/10.1016/j.scriptamat.2016.10.019>.
- Tomsett, D.I., Bevis, M. (1969). The formation of stacking faults in {10–12} twins in zinc as a result of slip dislocation-deformation twin interactions. *Philos. Mag. A* 19 (159), 533–537. <https://doi.org/10.1080/14786436908216310>.
- Tu, J., Zhang, S. (2016). On the {10–12} twinning growth mechanism in hexagonal close-packed metals. *Mater. Design* 96, 143–149. <https://doi.org/10.1016/j.matdes.2016.02.002>.
- Wang, H., Wang, Q.D., Boehlert, C.J., Yin, D.D., Yuan, J. (2015). Tensile and compressive creep behavior of extruded Mg–10Gd–3Y–0.5Zr (wt.%) alloy. *Mater. Charact.* 99, 25–37. <https://doi.org/10.1016/j.matchar.2014.11.006>.
- Wang, F., Agnew, S.R. (2016). Dislocation transmutation by tension twinning in magnesium alloy AZ31. *Int. J. Plasticity* 81, 63–86. <https://doi.org/10.1016/j.ijplas.2016.01.012>.
- Wu, D., Chen, R.S., Han, E.H. (2012). Serrated flow and tensile properties of a Mg–Gd–Zn alloy. *Mat. Sci. Eng. A-Struct.* 532, 267–274. <https://doi.org/10.1016/j.msea.2011.10.090>.
- Yuan, J., Wang, Q., Yin, D., Wang, H., Chen, C., Ye, B. (2013). Creep behavior of Mg–9Gd–1Y–0.5Zr (wt.%) alloy piston by squeeze casting. *Mater. Charact.* 78, 37–46. <https://doi.org/10.1016/j.matchar.2013.01.012>.
- Zhongjun, W., Weiping, J., Jianzhong, C. (2007). Study on the Deformation Behavior of Mg-3.6% Er Magnesium Alloy. *J. Rare Earth* 25 (6), 744–748. [https://doi.org/10.1016/S1002-0721\(08\)60019-8](https://doi.org/10.1016/S1002-0721(08)60019-8).
- Zhu, S.M., Nie, J.F. (2004). Serrated flow and tensile properties of a Mg–Y–Nd alloy. *Scripta Mater.* 50 (1), 51–55. <https://doi.org/10.1016/j.scriptamat.2003.09.039>.
- Zhu, S.M., Gibson, M.A., Easton, M.A., Nie, J.F. (2010). The relationship between microstructure and creep resistance in die-cast magnesium–rare earth alloys. *Scripta Mater.* 63 (7), 698–703. <https://doi.org/10.1016/j.scriptamat.2010.02.005>.
- Zhu, Y.M., Morton, A.J., Nie, J.F. (2012). Growth and transformation mechanisms of 18R and 14H in Mg–Y–Zn alloys. *Acta Mater.* 60 (19), 6562–6572. <https://doi.org/10.1016/j.actamat.2012.08.022>.
- Zhu, Y.M., Bian, M.Z., Nie, J.F. (2017). Tilt boundaries and associated solute segregation in a Mg-Gd alloy. *Acta Mater.* 127, 505–518. <https://doi.org/10.1016/j.actamat.2016.12.032>.
- Zhu, Y.M., Xu, S.W., Nie J.F. (2018). {1011} Twin boundary structure in a Mg-Gd alloy. *Acta Mater.* 143, 1–12. <https://doi.org/10.1016/j.actamat.2017.09.067>.